# AN IMPROVED STUDY OF THE STRUCTURE OF e⁺e⁻ → $b\bar{b}g$ EVENTS AND LIMITS ON THE ANOMALOUS CHROMOMAGNETIC COUPLING OF THE $b$-QUARK*

**The SLD Collaboration**∗∗
Stanford Linear Accelerator Center
Stanford University, Stanford, CA 94309

## ABSTRACT

The structure of three-jet e⁺e⁻ → $b\bar{b}g$ events has been studied using hadronic $Z^0$ decays recorded in the SLD experiment at SLAC. Three-jet final states were selected and the CCD-based vertex detector was used to identify two of the jets as $b$ or $\bar{b}$; the remaining jet in each event was tagged as the gluon jet. Distributions of the gluon energy and polar angle with respect to the electron beam were measured over the full kinematic range, and used to test the predictions of perturbative QCD. The energy distribution is potentially sensitive to an anomalous $b$ chromomagnetic moment $\kappa$ at the $b\bar{b}g$ vertex. We measured $\kappa$ to be consistent with zero and set 95% C.L. limits on its value, $-0.07 < \kappa < 0.08$ (preliminary).

*Contributed to: the International Europhysics Conference on High Energy Physics, 12–18 July, 2001, Budapest, Hungary, Ref: 667; and the XX$^{th}$ International Symposium on Lepton and Photon Interactions, 23–28 July, 2001, Rome, Italy*

# 1   Introduction

The observation of $e^+e^-$ annihilation into final states containing three hadronic jets, and their interpretation in terms of the process $e^+e^- \rightarrow q\overline{q}g$ [1], provided the first direct evidence for the existence of the gluon, the gauge boson of the theory of strong interactions, Quantum Chromodynamics (QCD). In subsequent studies the jets were usually energy ordered, and the lowest-energy jet was assigned as the gluon; this is correct roughly 80% of the time, but preferentially selects low-energy gluons. If the gluon jet could be tagged explicitly, event-by-event, the full kinematic range of gluon energies could be explored, and more detailed tests of QCD could be performed [2]. Due to advances in vertex-detection this is now possible using $e^+e^- \rightarrow b\overline{b}g$ events. The large mass and relatively long lifetime, $\sim 1.5$ ps, of the leading $B$ hadron in $b$-quark jets [3] lead to decay signatures that distinguish them from lighter-quark ($u$, $d$, $s$ or $c$) and gluon jets. We used the upgraded (1996-8) CCD vertex detector (VXD) [4] to identify in each event the two jets that contain the $B$ hadrons, and hence to tag the gluon jet. This allowed us to measure the gluon energy and polar-angle distributions over the full kinematic range.

Additional motivation to study the $b\overline{b}g$ system has been provided by measurements involving inclusive $Z^0 \rightarrow b\overline{b}$ decays. Several reported determinations [5] of $R_b = \Gamma(Z^0 \rightarrow b\overline{b})/\Gamma(Z^0 \rightarrow q\overline{q})$ and the $Z^0$-$b$ parity-violating coupling parameter, $A_b$, differed from Standard Model (SM) expectations at the few standard deviation level. Since one expects new high-mass-scale dynamics to couple to the massive third-generation fermions, these measurements aroused considerable interest and speculation. We have therefore investigated in detail the strong-interaction dynamics of the $b$-quark. We have compared the strong coupling of the gluon to $b$-quarks with that to light- and charm-quarks [6], as well as tested parity (P) and charge$\oplus$parity (CP) conservation at the $b\overline{b}g$ vertex [7]. We have also studied the structure of $b\overline{b}g$ events, via the distributions of the gluon energy and polar angle with respect to (w.r.t.) the beamline [8], using the JADE algorithm [9] for jet definition. Here we present a preliminary update of these measurements using a data sample more than 3 times larger than in our earlier study, and using in addition the Durham, Geneva, E, E0 and P algorithms [10] to define jets. We compare these results with perturbative QCD predictions.

In QCD the chromomagnetic moment of the $b$ quark is induced at the one-loop level

| Jet algorithm | $y_c$ value | # 3-jet events |
|:---:|:---:|:---:|
| JADE | 0.025 | 57341 |
| Durham | 0.0095 | 46432 |
| E | 0.0275 | 66848 |
| E0 | 0.0275 | 54163 |
| P | 0.02 | 60387 |
| Geneva | 0.05 | 40895 |

Table 1: Number of selected 3-jet events for each algorithm.

and is of order $\alpha_s/\pi$. A more general $b\bar{b}g$ Lagrangian term with a modified coupling [11] may be written:

$$\mathcal{L}^{b\bar{b}g} = g_s \bar{b} T_a \{ \gamma_\mu + \frac{i\sigma_{\mu\nu}k^\nu}{2m_b}(\kappa - i\tilde{\kappa}\gamma_5) \} b G_a^\mu, \tag{1}$$

where $\kappa$ and $\tilde{\kappa}$ parameterize the anomalous chromomagnetic and chromoelectric moments, respectively, which might arise from physics beyond the SM. The effects of the chromoelectric moment are sub-leading w.r.t. those of the chromomagentic moment, so for convenience we set $\tilde{\kappa}$ to zero. A non-zero $\kappa$ would be observable as a modification [11] of the gluon energy distribution in $b\bar{b}g$ events relative to the standard QCD case. By measuring this distribution precisely, we have set tight limits on $\kappa$.

## 2 $b\bar{b}g$ Event Selection

We used hadronic decays of $Z^0$ bosons produced by $e^+e^-$ annihilations at the SLAC Linear Collider (SLC) and recorded in the SLC Large Detector (SLD) [12]. The criteria for selecting hadronic $Z^0$ decays and the charged tracks used for flavor-tagging are described in [6, 13]. Three-jet events were selected using iterative clustering algorithms applied to the set of charged tracks in each event. We used in turn the JADE, Durham, E, E0, P and Geneva algorithms; the respective scaled-invariant-mass, $y_{cut}$, values used are shown in Table 1.

Events classified as 3-jet states were retained if all three jets were well contained within the barrel tracking system, with polar angle $|\cos\theta_{jet}| \leq 0.80$. In addition, in order to select planar 3-jet events, the sum of the angles between the jet axes

was required to be between 358 and 360 degrees. From our 1996-98 data samples, comprising roughly 400,000 hadronic $Z^0$ decays, the numbers of selected events are shown in Table 1. In order to improve the energy resolution the jet energies were rescaled kinematically according to the angles between the jet axes, assuming energy and momentum conservation and massless kinematics. The jets were then labelled in order of energy such that $E_1 > E_2 > E_3$.

Charged tracks with high quality information in the VXD [6] were used to tag $b\bar{b}g$ events. The resolution on the impact parameter $d$ is given by $\sigma_d = 7.7 \oplus 29/p \sin^{3/2} \theta$ $\mu$m in the plane transverse to the beamline, and $9.6 \oplus 29/p \sin^{3/2} \theta$ $\mu$m in any plane containing the beamline, where $p$ is the track momentum in GeV/c, and $\theta$ the polar angle, w.r.t. the beamline. Jets containing heavy hadrons were tagged using a topological algorithm [14] applied to the set of tracks in the jet. A track density function was calculated, and regions of high total track density well separated from the interaction point (IP) were identified as secondary vertices from the decay of a heavy hadron. For each vertex, the $p_t$-corrected invariant mass [14] was calculated from the set of tracks attached to the vertex, assuming the charged pion mass, and the vertex axis (direction from the IP to the reconstructed vertex position). Events were retained in which exactly two jets contained such a vertex, and at least one of them had a $p_t$-corrected mass greater than 2 GeV/c$^2$. In each tagged event the jet without a vertex was tagged as the gluon jet. For each algorithm, the number of tagged jets is shown in Tables 2,3,4,5,6,7; also shown is the overall efficiency for gluon-jet selection, which was calculated using a simulated event sample generated with JETSET 7.4 [15], with parameter values tuned to hadronic $e^+e^-$ annihilation data [16], combined with a simulation of $B$-decays tuned to $\Upsilon(4S)$ data [17] and a simulation of the detector. The efficiency peaks at about 16% for 18 GeV gluons. Lower-energy gluon jets are sometimes merged with the parent $b$-jet by the jet-finder. At higher gluon energies the correspondingly lower-energy $b$-jets are harder to tag, and there is also a higher probability of losing a jet outside the detector acceptance.

For the selected event sample, Fig. 1 shows the $M_{pt}$ distributions separately for vertices found in jets 1, 2 and 3 using, for illustration, the JADE algorithm; results using the other algorithms (not shown) are qualitatively similar. The simulated contributions from true $b$-, $c$, light- and gluon-jets are indicated [18]. For each algorithm the purities [18] are listed by jet number in Tables 2,3,4,5,6,7. We formed the distributions

4

| JADE | efficiency = | 12.3% |
|---|---|---|
| Jet label | # Tagged gluon jets | Purity |
| 3 | 4384 | 82.1 % |
| 2 | 761 | 79.1 % |
| 1 | 190 | 63.7 % |

Table 2: Estimated purities of the tagged gluon-jet samples defined using the JADE algorithm.

| Durham | efficiency = | 12.2% |
|---|---|---|
| Jet label | # Tagged gluon jets | Purity |
| 3 | 2983 | 78.2 % |
| 2 | 910 | 74.0 % |
| 1 | 173 | 64.9 % |

Table 3: Estimated purities of the tagged gluon-jet samples defined using the Durham algorithm.

| E | efficiency = | 11.9% |
|---|---|---|
| Jet label | # Tagged gluon jets | Purity |
| 3 | 5288 | 77.7 % |
| 2 | 1031 | 63.2 % |
| 1 | 184 | 52.0 % |

Table 4: Estimated purities of the tagged gluon-jet samples defined using the E algorithm.

| E0 | efficiency = | 11.4% |
|---|---|---|
| Jet label | # Tagged gluon jets | Purity |
| 3 | 4061 | 83.5 % |
| 2 | 712 | 81.3 % |
| 1 | 194 | 62.2 % |

Table 5: Estimated purities of the tagged gluon-jet samples defined using the E0 algorithm.

| P | efficiency = | 11.3% |
|---|---|---|
| Jet label | # Tagged gluon jets | Purity |
| 3 | 4691 | 82.3 % |
| 2 | 816 | 77.1 % |
| 1 | 198 | 60.0 % |

Table 6: Estimated purities of the tagged gluon-jet samples defined using the P algorithm.

| Geneva | efficiency = | 13.0% |
|---|---|---|
| Jet label | # Tagged gluon jets | Purity |
| 3 | 3526 | 67.9 % |
| 2 | 708 | 69.3 % |
| 1 | 228 | 51.6 % |

Table 7: Estimated purities of the tagged gluon-jet samples defined using the Geneva algorithm.

of two gluon-jet observables, the scaled energy $x_g = 2E_{\mathrm{gluon}}/\sqrt{s}$, and the polar angle w.r.t. the beamline, $\theta_g$. For illustration, for the JADE algorithm the distributions are shown in Fig. 2; the simulation is also shown; it reproduces the data. Results for the other algorithms (not shown) are qualitatively similar.

The backgrounds were estimated using the simulation and are of three types: non-$b\bar{b}$ events; $b\bar{b}$ but non-$b\bar{b}g$ events; and mis-tagged events. These are shown in Fig. 2 for the JADE case. The non-$b\bar{b}$ events ($\sim$1% of the selected sample) are mainly (95%) $c\bar{c}g$ events, most of which had the gluon jet correctly tagged. Mis-tagged events, in which the gluon jet was mis-tagged as a $b/\bar{b}$-jet and the $b$ or $\bar{b}$ jet enters into the measured distributions, comprise roughly 2% of the total sample. These two backgrounds are negligible except in the highest $x_g$ bin. The dominant background (16% of the sample) is formed by $b\bar{b}$ but non-$b\bar{b}g$ events. These are true $b\bar{b}$ events that were not classified as 3-jet events at the parton level, but were poorly reconstructed and tagged as 3-jet $b\bar{b}g$ events in the detector using the same jet algorithm and $y_{cut}$ value. At low gluon energy, this arises from the broadening of the particle flow around the original $b$ and $\bar{b}$ directions due to hadronization, especially the relatively high-transverse-momentum $B$-decay products, which can cause the jet-finder to reconstruct a 'fake' third jet, almost always assigned as the gluon. At high gluon energy, an event classified as 4-jet at the parton level may have two of its jets combined by the jet-finder, due to the overlap of their hadronization products. In this case the tagged jet is usually a gluon jet or pair of gluon jets, however since the calculations with which we compare below are not reliable for 4-jet events, we consider them a background. Results for the other algorithms (not shown) are similar.

# 3    Correction of the Data

For each algorithm, the distributions were corrected to obtain the true gluon distributions $D^{true}(X)$ by applying a bin-by-bin procedure: $D^{true}(X) = C(X)\,(D^{raw}(X) - B(X))$, where $X = x_g$ or $\cos\theta_g$, $D^{raw}(X)$ is the raw distribution, $B(X)$ is the background contribution, and $C(X) \equiv D^{true}_{MC}(X)/D^{recon}_{MC}(X)$ is a correction that accounts for the efficiency for accepting true $b\bar{b}g$ events into the tagged sample, as well as for bin-to-bin migrations caused by hadronization, the resolution of the detector, and bias of the jet-tagging technique. Here $D^{true}_{MC}(X)$ is the true distribution for MC-generated
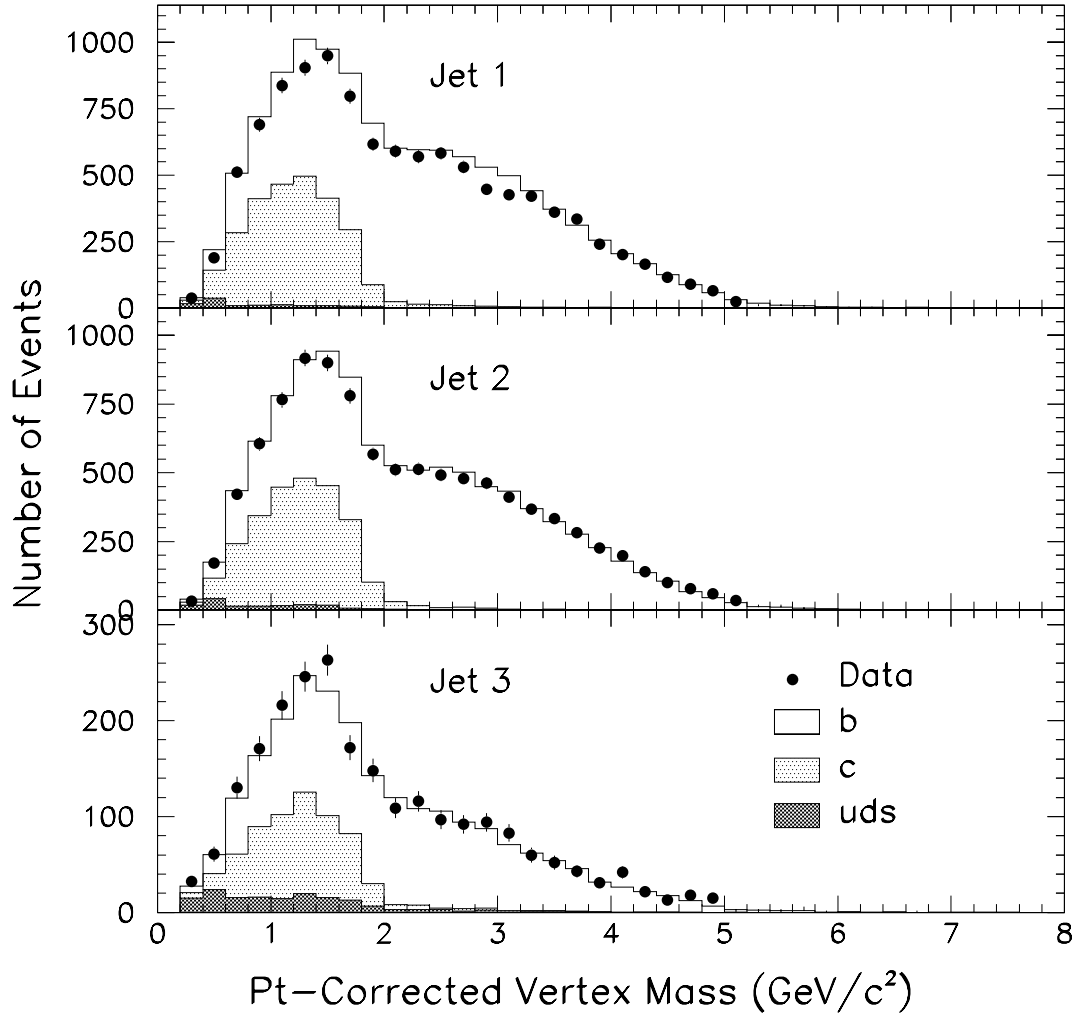
Figure 1: The $M_{pt}$ distributions for vertices found in $b\bar{b}g$-tagged events, defined using the JADE algorithm, labelled according to jet energy (dots); errors are statistical. Histograms: simulated distributions for different jet flavors.
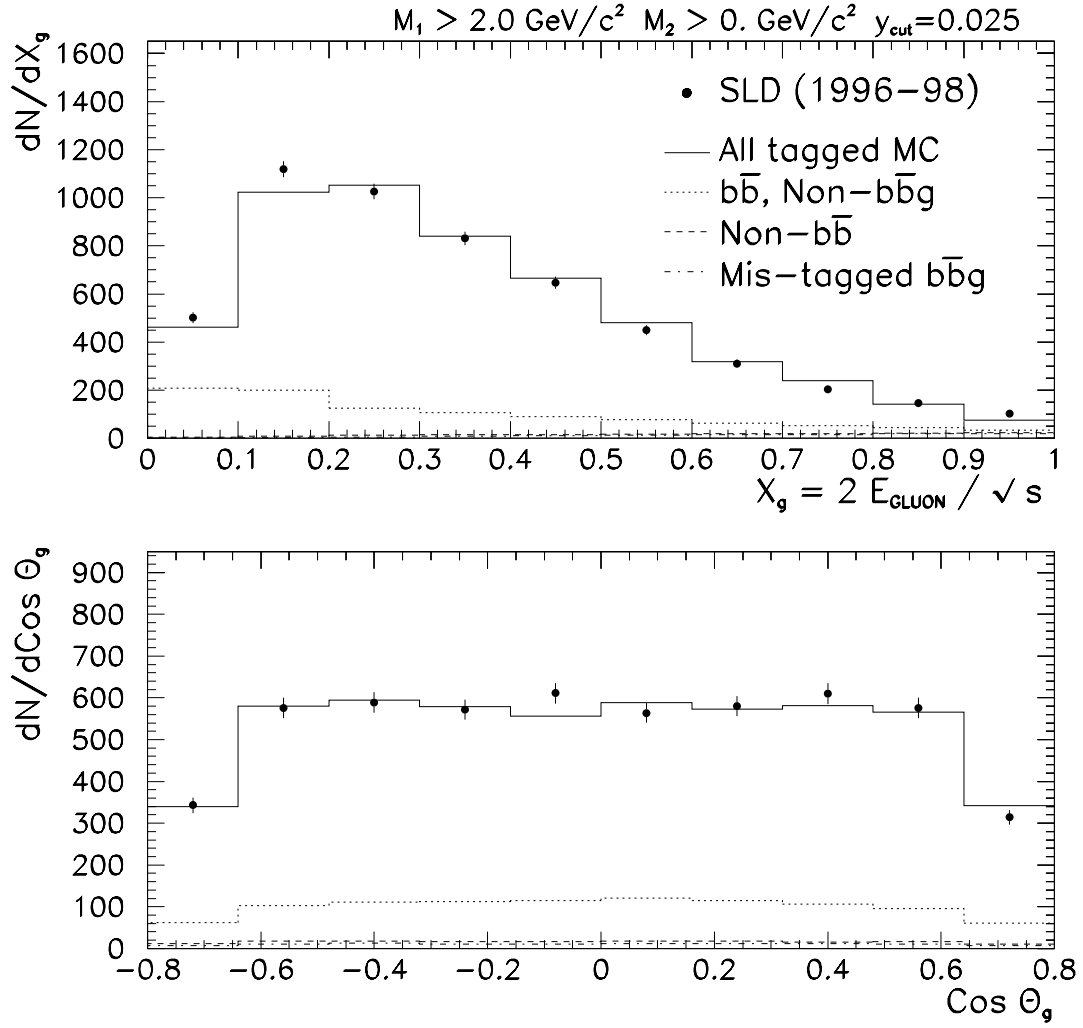
Figure 2: Raw measured distributions of (a) $x_g$ and (b) $\cos\theta_g$ (dots) defined using the JADE algorithm; errors are statistical. Histograms: simulated distributions including background contributions.

$b\bar{b}g$ events, and $D_{MC}^{recon}(X)$ is the resulting distribution after full simulation of the detector and application of the same analysis procedure as applied to the data.

As a cross-check, an alternative correction procedure was employed in which bin-to-bin migrations, which can be as large as 20%, were explicitly taken into account: $D^{true}(X_i) = M(X_i, X_j)(D^{raw}(X_j) - B(X_j))/\epsilon(X_i)$, with the unfolding matrix $M(X_i, X_j)$ defined by $D_{MC}^{true}(X_i) = M(X_i, X_j)D_{MC}^{recon}(X_j)$, where true $b\bar{b}g$ events generated in bin $i$ may, after reconstruction, be accepted into the tagged sample in bin $j$. $\epsilon(X)$ is the efficiency for accepting $b\bar{b}g$ events in bin $i$ into the tagged sample. The resulting distributions of $x_g$ and $\cos\theta_g$ are statistically indistinguishable from the respective distributions yielded by the bin-by-bin method.

The fully-corrected distributions are shown in Figs. 3,4,5,6,7,8. Since, in an earlier study [6], we verified that the overall rate of $b\bar{b}g$-event production is consistent with QCD expectations, we normalised the gluon distributions to unit area and we study further the distribution shapes. In each case the peak in $x_g$ is a kinematic artefact of the jet-finding algorithm, which ensures that gluon jets are reconstructed with a non-zero energy and depends on the $y_c$ value. The $\cos\theta_g$ distribution is very nearly flat, in contrast to the $1 + \cos^2\theta$ behaviour for quark jets.

We have considered sources of systematic uncertainty that potentially affect our results. These may be divided into uncertainties in modelling the detector and uncertainties in the underlying physics modelling. To estimate the first case we systematically varied the track and event selection requirements, as well as the trackfinding efficiency [6, 13], the momentum and dip angle resolution, and the probability of finding a fake vertex in a jet. In the second case parameters used in our simulation, relating mainly to the production and decay of charm and bottom hadrons, were varied within their measurement errors [13]. For each variation the data were recorrected to derive new $x_g$ and $\cos\theta_g$ distributions, and the deviation w.r.t. the standard case was assigned as a systematic uncertainty. Although many of these variations affect the overall tagging efficiency, most had little effect on the energy or polar angle dependence, and no variation affects the conclusions below. All uncertainties were conservatively assumed to be uncorrelated and were added in quadrature in each bin of $x_g$ and $\cos\theta_g$.
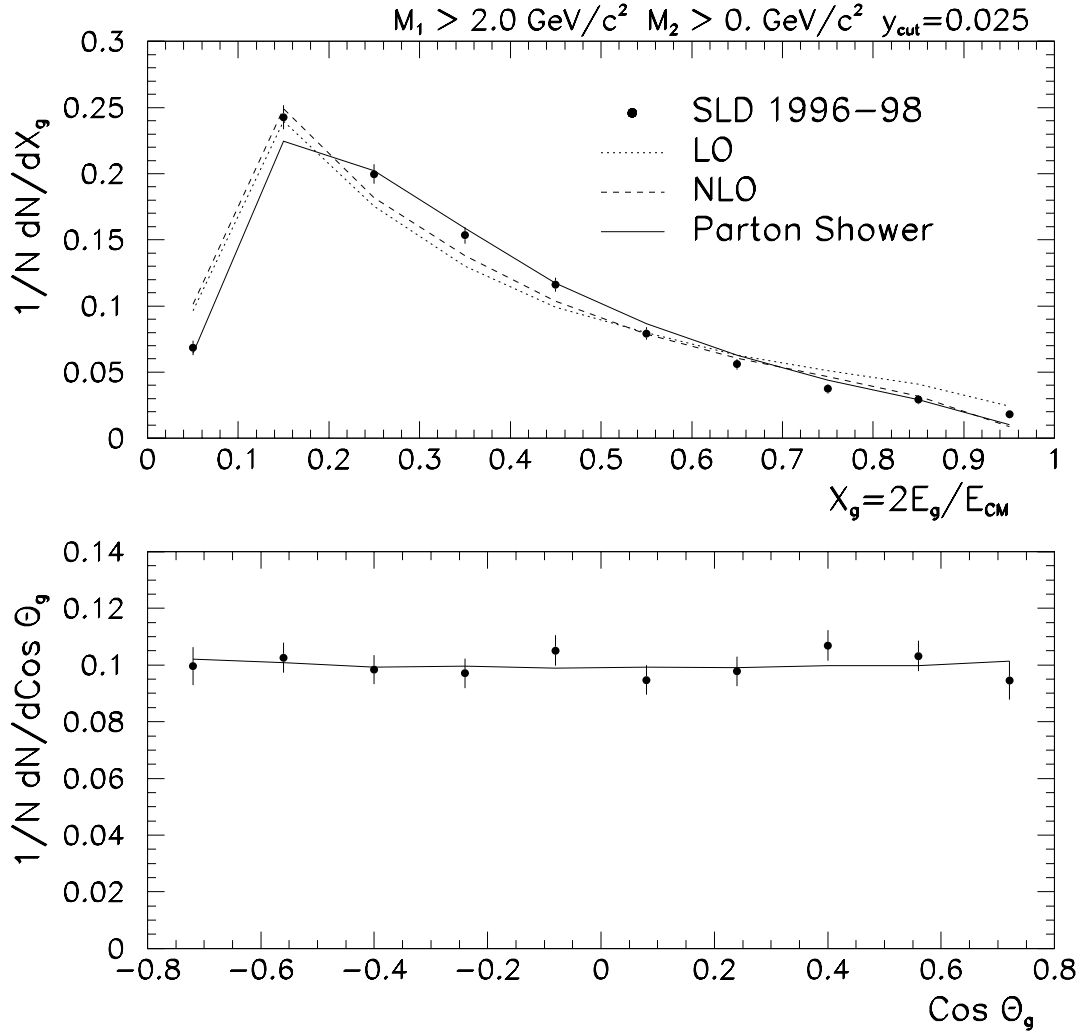
Figure 3: Corrected distributions of (a) $x_g$ and (b) $\cos\theta_g$ (dots) defined using the JADE algorithm; errors are statistical. Perturbative QCD predictions (see text) are shown as lines joining entries plotted at the respective bin centers.
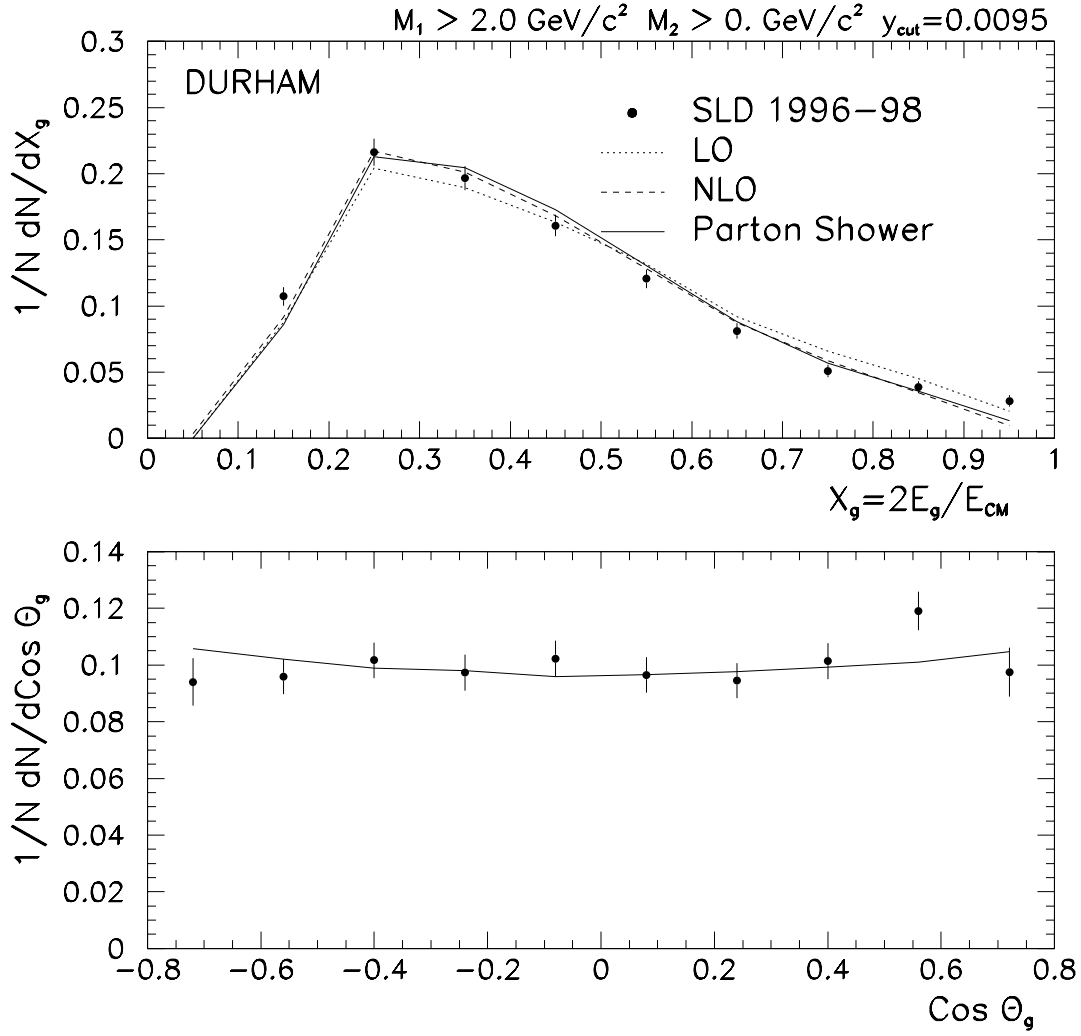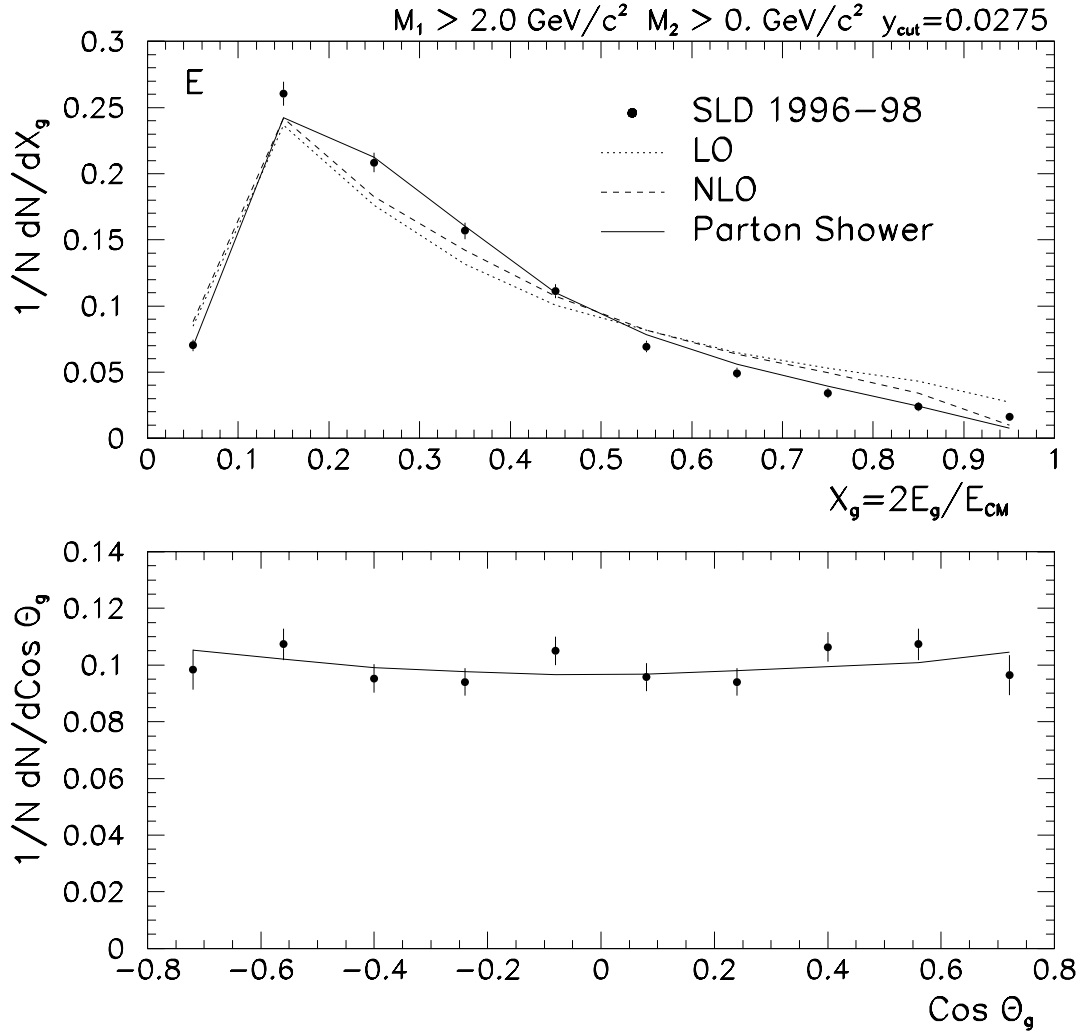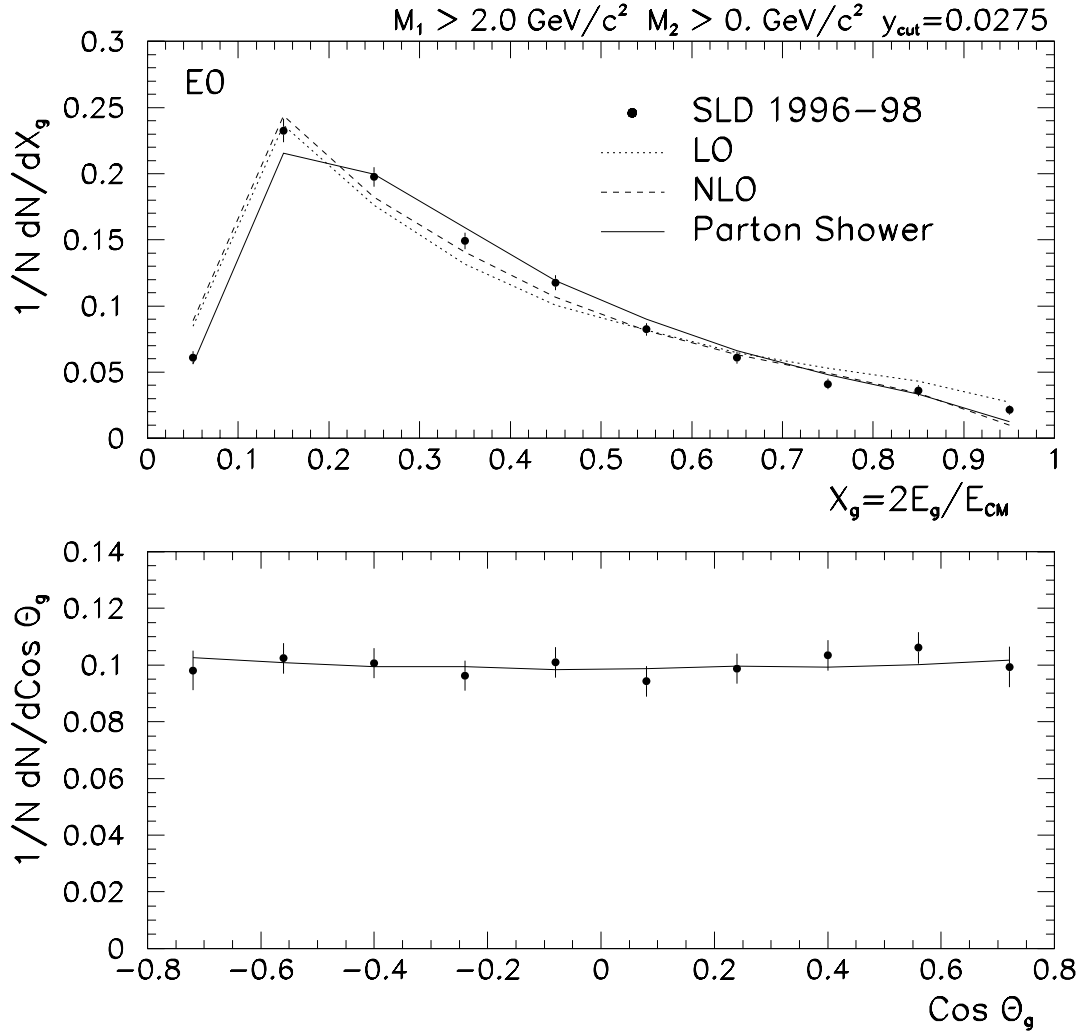
Figure 4: Corrected distributions of (a) $x_g$ and (b) $\cos\theta_g$ (dots); defined using the Durham algorithm; errors are statistical. Perturbative QCD predictions (see text) are shown as lines joining entries plotted at the respective bin centers.

Figure 5: Corrected distributions of (a) $x_g$ and (b) $\cos\theta_g$ (dots); defined using the E algorithm; errors are statistical. Perturbative QCD predictions (see text) are shown as lines joining entries plotted at the respective bin centers.
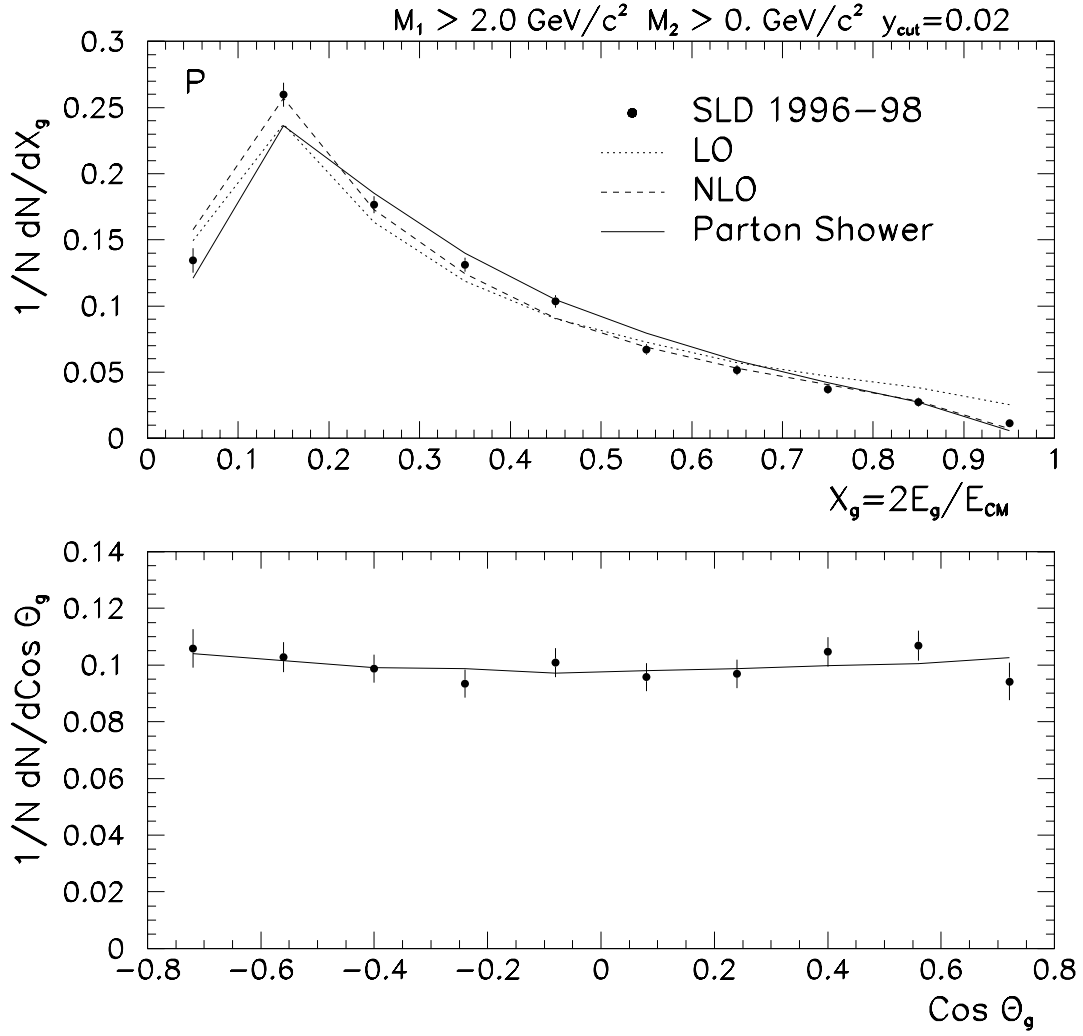
13

Figure 6: Corrected distributions of (a) $x_g$ and (b) $\cos\theta_g$ (dots); defined using the E0 algorithm; errors are statistical. Perturbative QCD predictions (see text) are shown as lines joining entries plotted at the respective bin centers.
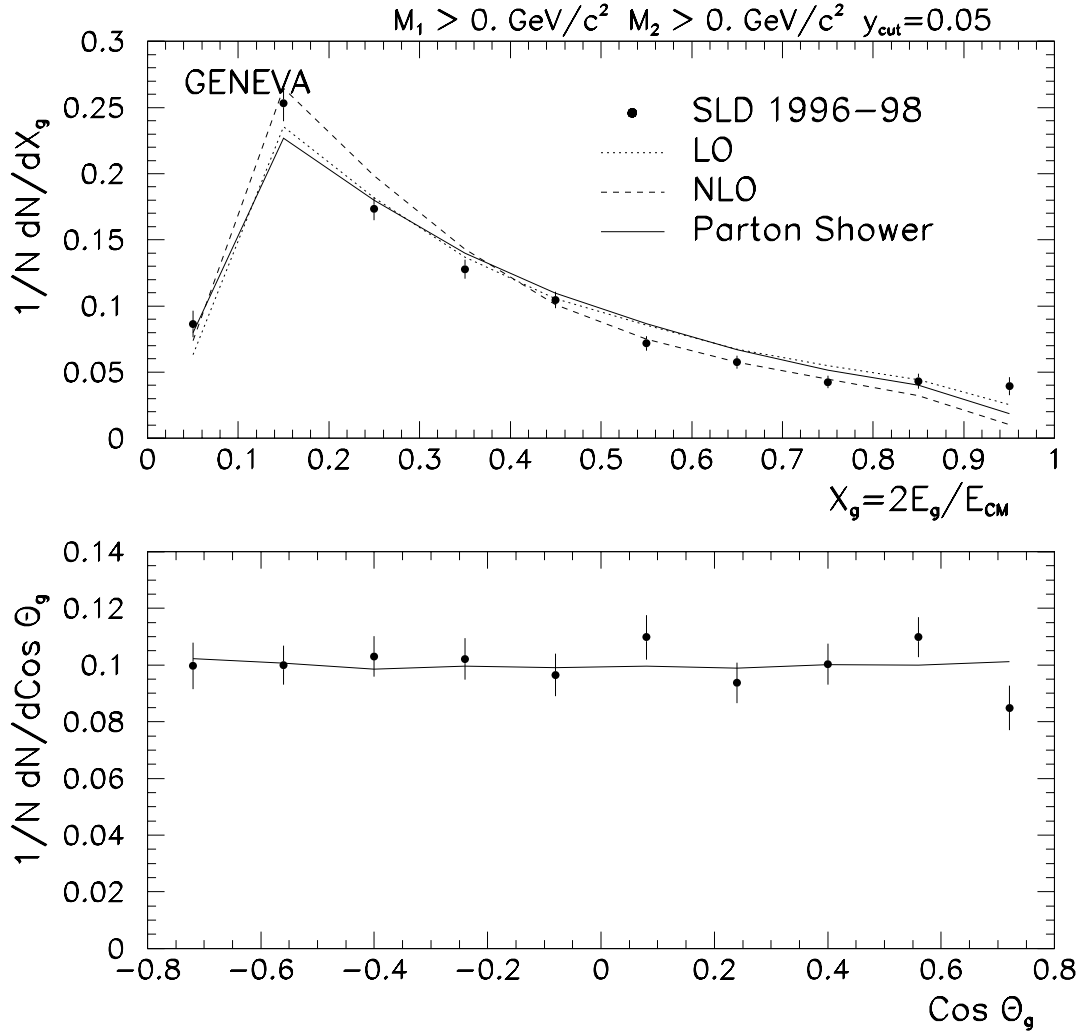
Figure 7: Corrected distributions of (a) $x_g$ and (b) $\cos\theta_g$ (dots); defined using the P algorithm; errors are statistical. Perturbative QCD predictions (see text) are shown as lines joining entries plotted at the respective bin centers.

Figure 8: Corrected distributions of (a) $x_g$ and (b) $\cos\theta_g$ (dots); defined using the Geneva algorithm; errors are statistical. Perturbative QCD predictions (see text) are shown as lines joining entries plotted at the respective bin centers.

# 4    Comparison with QCD Predictions

We compared the data with perturbative QCD predictions for the respective jet algorithm and $y_c$ value. We calculated leading-order (LO) and NLO results using JETSET. We also derived these distributions using the 'parton shower' (PS) implemented in JETSET. This is equivalent to a calculation in which all leading, and a subset of next-to-leading, $\ln y_c$ terms are resummed to all orders in $\alpha_s$. In physical terms this allows events to be generated with multiple orders of parton radiation, in contrast to the maximum number of 3 (4) partons allowed in the LO (NLO) calculations, respectively. Configurations with $\geq 3$ partons are relevant to the observables considered here since they may be resolved as 3-jet events by the jet-finding algorithm.

These predictions are shown in Figs. 3,4,5,6,7,8. For illustration we discuss the JADE case. The three calculations are indistinguishable for the $\cos\theta_g$ distributions and reproduce the measured distribution, which is almost flat and insensitive to the details of higher order soft parton emission. For $x_g$, the LO calculation reproduces the main features of the shape of the distribution, but yields too few events in the region $0.2 < x_g < 0.5$, and too many events for $x_g < 0.1$ and $x_g > 0.6$. The NLO calculation is noticeably better, but shows qualitatively similar deficiencies. The PS calculation describes the data reasonably across the full $x_g$ range. These results suggest that multiple orders of parton radiation need to be included, in agreement with our earlier measurements of jet energy distributions using flavor-inclusive $Z^0$ decays [19]. Results for the other algorithms are qualitatively similar.

We conclude that perturbative QCD in the PS approximation reproduces the gluon distributions in $b\bar{b}g$ events. However, it is interesting to consider the extent to which anomalous chromomagnetic contributions are allowed by the data. The Lagrangian represented by Eq. 1 yields a model that is non-renormalizable. Nevertheless tree-level predictions can be derived [11] and used for a 'straw man' comparison with QCD. For each jet algorithm, in each bin of the $x_g$ distribution, we parametrised the leading-order effect of an anomalous chromomagnetic moment and added it to the PS calculation to arrive at an effective QCD prediction including the anomalous moment at leading-order. A $\chi^2$ minimization fit was performed to the data with $\kappa$ as a free parameter. The corresponding $\kappa$ and $\chi^2$ values are shown in Table 8. For each algorithm the $x_g$ distribution corresponding to the fit is indistinguishable from the respective PS predic-

17

| Jet algorithm | $\kappa$ | $\chi^2$: $x_g$ (10 bins) | 95% C.L. limits |
|---|---|---|---|
| JADE | $0.003 \pm 0.032$ | 21.6 | $-0.07 < \kappa < 0.08$ |
| Durham | $0.055 \pm 0.036$ | 27.7 | $-0.03 < \kappa < 0.14$ |
| E | $0.009 \pm 0.030$ | 24.3 | $-0.06 < \kappa < 0.08$ |
| E0 | $0.006 \pm 0.033$ | 21.5 | $-0.07 < \kappa < 0.08$ |
| P | $0.023 \pm 0.028$ | 38.6 | $-0.04 < \kappa < 0.09$ |
| Geneva | $0.000 \pm 0.030$ | 32.4 | $-0.07 < \kappa < 0.07$ |

Table 8: Best-fit $\kappa$ values and 95% C.L. limits.

tion. In all cases $\kappa$ is consistent with zero, and the corresponding 95% confidence-level (C.L.) limits on its value are shown in Table 8. Since the results are rather correlated, we quote preliminary limits on $\kappa$ using the JADE algorithm, yielding $-0.07 < \kappa < 0.08$ at the 95% C.L.

# 5   Conclusion

In conclusion, we used the precise SLD tracking system to tag the gluon in 3-jet $e^+e^- \rightarrow Z^0 \rightarrow b\bar{b}g$ events. We studied the structure of these events in terms of the scaled gluon energy and polar angle, measured across the full kinematic range. We compared our data with perturbative QCD predictions, and found that the effect of the $b$-mass on the shapes of the distributions is small, that beyond-LO QCD contributions are needed to describe the energy distribution, and that the parton shower prediction agrees with the data. We also investigated an anomalous $b$-quark chromomagnetic moment, $\kappa$, which would affect the shape of the energy distribution. We set preliminary 95% c.l. limits of $-0.07 < \kappa < 0.08$ (preliminary).

# References

[1] See *eg.* S.L. Wu, Phys. Rept. **107** (1984) 59.
J. Ellis, M. K. Gaillard, and G. G. Ross, Nucl. Phys. **B111** (1976) 253; erratum: *ibid.* **B130** (1977) 516.

[2] See *eg.* P.N. Burrows, P. Osland, Phys. Lett. **B400** (1997) 385.

[3] We do not distinguish between particle and antiparticle.

[4] K. Abe *et al.*, Nucl. Inst. Meth. **A400** (1997) 287.

[5] See *eg.*, G. C. Ross, Electroweak Interactions and Unified Theories, Proc. xXXXI Rencontre de Moriond, 16-23 March 1996, Les Arcs, Savoie, France, Editions Frontieres (1996), ed. J. Tran Thanh Van, p 481.

[6] SLD Collab., K. Abe *et al.*, Phys. Rev. **D59** (1999) 012002.

[7] SLD Collab., Koya Abe *et al.*, Phys. Rev. Lett. **86** (2001) 962.

[8] SLD Collab., K. Abe *et al.*, Phys. Rev. **D60** (1999) 92002.

[9] JADE Collab., W. Bartel *et. al.*, Z. Phys. **C33** (1986) 23.

[10] See *eg.*, SLD Collab., K. Abe *et al.*, Phys. Rev. **D51** (1995) 962.

[11] T. Rizzo, Phys. Rev. **D50** (1994) 4478, and private communications.

[12] SLD Design Report, SLAC Report 273 (1984).

[13] P.J. Dervan, Brunel Univ. Ph.D. thesis; SLAC-Report-523 (1998).

[14] D.J. Jackson, Nucl. Instrum. Meth. **A388** (1997) 247.

[15] T. Sjöstrand, Comp. Phys. Commun. **82** (1994) 74.

[16] P. N. Burrows, Z. Phys. **C41** (1988) 375.
     OPAL Collab., M. Z. Akrawy *el al.*, *ibid.* **C47** (1990) 505.

[17] SLD Collab., K. Abe *et al.*, Phys. Rev. Lett. **79** (1997) 590.

[18] We expect less than 0.4% of the selected sample to comprise events of the type $e^+e^- \rightarrow q\bar{q}g$, with $g \rightarrow b\bar{b}$. In the evaluation of the purity only true $b\bar{b}\,b\bar{b}$ events were considered as signal $b\bar{b}g$ events; $q\bar{q}\,b\bar{b}$ events ($q \neq b$) were considered as backgrounds.

[19] SLD Collab., K. Abe *et al.*, Phys. Rev. **D55**, (1997) 2533.

# **List of Authors

Koya Abe,[24] Kenji Abe,[15] T. Abe,[21] I. Adam,[21] H. Akimoto,[21] D. Aston,[21]
K.G. Baird,[11] C. Baltay,[30] H.R. Band,[29] T.L. Barklow,[21] J.M. Bauer,[12]
G. Bellodi,[17] R. Berger,[21] G. Blaylock,[11] J.R. Bogart,[21] G.R. Bower,[21]
J.E. Brau,[16] M. Breidenbach,[21] W.M. Bugg,[23] D. Burke,[21] T.H. Burnett,[28]
P.N. Burrows,[17] A. Calcaterra,[8] R. Cassell,[21] A. Chou,[21] H.O. Cohn,[23]
J.A. Coller,[4] M.R. Convery,[21] V. Cook,[28] R.F. Cowan,[13] G. Crawford,[21]
C.J.S. Damerell,[19] M. Daoudi,[21] N. de Groot,[2] R. de Sangro,[8] D.N. Dong,[13]
M. Doser,[21] R. Dubois, I. Erofeeva,[14] V. Eschenburg,[12] E. Etzion,[29] S. Fahey,[5]
D. Falciai,[8] J.P. Fernandez,[26] K. Flood,[11] R. Frey,[16] E.L. Hart,[23]
K. Hasuko,[24] S.S. Hertzbach,[11] M.E. Huffer,[21] X. Huynh,[21] M. Iwasaki,[16]
D.J. Jackson,[19] P. Jacques,[20] J.A. Jaros,[21] Z.Y. Jiang,[21] A.S. Johnson,[21]
J.R. Johnson,[29] R. Kajikawa,[15] M. Kalelkar,[20] H.J. Kang,[20] R.R. Kofler,[11]
R.S. Kroeger,[12] M. Langston,[16] D.W.G. Leith,[21] V. Lia,[13] C. Lin,[11]
G. Mancinelli,[20] S. Manly,[30] G. Mantovani,[18] T.W. Markiewicz,[21]
T. Maruyama,[21] A.K. McKemey,[3] R. Messner,[21] K.C. Moffeit,[21] T.B. Moore,[30]
M. Morii,[21] D. Muller,[21] V. Murzin,[14] S. Narita,[24] U. Nauenberg,[5] H. Neal,[30]
G. Nesom,[17] N. Oishi,[15] D. Onoprienko,[23] L.S. Osborne,[13] R.S. Panvini,[27]
C.H. Park,[22] I. Peruzzi,[8] M. Piccolo,[8] L. Piemontese,[7] R.J. Plano,[20]
R. Prepost,[29] C.Y. Prescott,[21] B.N. Ratcliff,[21] J. Reidy,[12] P.L. Reinertsen,[26]
L.S. Rochester,[21] P.C. Rowson,[21] J.J. Russell,[21] O.H. Saxton,[21] T. Schalk,[26]
B.A. Schumm,[26] J. Schwiening,[21] V.V. Serbo,[21] G. Shapiro,[10] N.B. Sinev,[16]
J.A. Snyder,[30] H. Staengle,[6] A. Stahl,[21] P. Stamer,[20] H. Steiner,[10] D. Su,[21]
F. Suekane,[24] A. Sugiyama,[15] A. Suzuki,[15] M. Swartz,[9] F.E. Taylor,[13]
J. Thom,[21] E. Torrence,[13] T. Usher,[21] J. Va'vra,[21] R. Verdier,[13]
D.L. Wagner,[5] A.P. Waite,[21] S. Walston,[16] A.W. Weidemann,[23] E.R. Weiss,[28]
J.S. Whitaker,[4] S.H. Williams,[21] S. Willocq,[11] R.J. Wilson,[6]
W.J. Wisniewski,[21] J.L. Wittlin,[11] M. Woods,[21] T.R. Wright,[29]
R.K. Yamamoto,[13] J. Yashima,[24] S.J. Yellin,[25] C.C. Young,[21] H. Yuta.[1]

[1]*Aomori University, Aomori, 030 Japan,*
[2]*University of Bristol, Bristol, United Kingdom,*
[3]*Brunel University, Uxbridge, Middlesex, UB8 3PH United Kingdom,*
[4]*Boston University, Boston, Massachusetts 02215,*
[5]*University of Colorado, Boulder, Colorado 80309,*
[6]*Colorado State University, Ft. Collins, Colorado 80523,*
[7]*INFN Sezione di Ferrara and Universita di Ferrara, I-44100 Ferrara, Italy,*
[8]*INFN Laboratori Nazionali di Frascati, I-00044 Frascati, Italy,*
[9]*Johns Hopkins University, Baltimore, Maryland 21218-2686,*
[10]*Lawrence Berkeley Laboratory, University of California, Berkeley, California
94720,*
[11]*University of Massachusetts, Amherst, Massachusetts 01003,*
[12]*University of Mississippi, University, Mississippi 38677,*

$^{(13)}$*Massachusetts Institute of Technology, Cambridge, Massachusetts 02139,*
$^{(14)}$*Institute of Nuclear Physics, Moscow State University, 119899 Moscow, Russia,*
$^{(15)}$*Nagoya University, Chikusa-ku, Nagoya, 464 Japan,*
$^{(16)}$*University of Oregon, Eugene, Oregon 97403,*
$^{(17)}$*Oxford University, Oxford, OX1 3RH, United Kingdom,*
$^{(18)}$*INFN Sezione di Perugia and Universita di Perugia, I-06100 Perugia, Italy,*
$^{(19)}$*Rutherford Appleton Laboratory, Chilton, Didcot, Oxon OX11 0QX United Kingdom,*
$^{(20)}$*Rutgers University, Piscataway, New Jersey 08855,*
$^{(21)}$*Stanford Linear Accelerator Center, Stanford University, Stanford, California 94309,*
$^{(22)}$*Soongsil University, Seoul, Korea 156-743,*
$^{(23)}$*University of Tennessee, Knoxville, Tennessee 37996,*
$^{(24)}$*Tohoku University, Sendai, 980 Japan,*
$^{(25)}$*University of California at Santa Barbara, Santa Barbara, California 93106,*
$^{(26)}$*University of California at Santa Cruz, Santa Cruz, California 95064,*
$^{(27)}$*Vanderbilt University, Nashville,Tennessee 37235,*
$^{(28)}$*University of Washington, Seattle, Washington 98105,*
$^{(29)}$*University of Wisconsin, Madison,Wisconsin 53706,*
$^{(30)}$*Yale University, New Haven, Connecticut 06511.*